LOW-VELOCITY IMPACT DAMAGE SIMULATION USING COHESIVE ZONE MODEL AND LARC05 CRITERION WITH EFFICIENT SEARCH ALGORITHM

P. Shabani[1], L. Li[2*], J. Laliberte[3**], G. Qi[2]
[1] Carleton University, PhD Student, Ottawa, Canada, [2] National Research Council Canada, Senior Research Officer, Ottawa, Canada, [3] Carleton University, Professor, Ottawa, Canada
* Corresponding author (Lucy.Li@nrc-cnrc.ca)
** Corresponding author (Jeremy.Laliberte@carleton.ca)

Keywords: *Composite laminates, Impact damage, Cohesive Zone Modelling*

ABSTRACT

A three-dimensional (3-D) finite element (FE) model was developed to accurately predict ply-by-ply damage sizes and failure modes interactions in a composite laminate after a low-velocity impact (LVI) event. To predict different failure modes, the cohesive zone modelling (CZM) technique and the LaRC05 failure criteria were employed. Cohesive layers were deployed between each adjacent composite ply to predict delamination. In addition, cohesive elements were embedded inside the composite plies to predict the delamination and matrix cracking interactions and delamination migration from one layer to another. The LaRC05 failure criteria were employed using a VUMAT user-defined material subroutine in Abaqus to account for matrix cracking, fibre breakage, fibre splitting, and fibre kinking. However, the need to find the matrix fracture plane (α) and fibre kink band angle (ψ) made the LaRC05 failure criteria 122% slower than the 3-D Hashin criteria in the impact simulation. To reduce the time required to find α and ψ, the Selective Range Golden Section Search (SRGSS) algorithm was used to efficiently find these angles. Using the SRGSS algorithm, α and ψ were found with a 1° precision 48% faster than the model without this search algorithm, and it was only 14% slower than the 3-D Hashin criteria. The LaRC05 criteria with the SRGSS algorithm captured well a realistic representation of angled intralaminar matrix cracking and failure mode interactions while improving the computational efficiency.

1 INTRODUCTION

Low-velocity impact (LVI) events can occur during the fabrication, service, and maintenance of composite airframes. The LVI may result in widespread internal damage and severe reduction in the strength and stability of the structure but the damage can be hard to detect. To support the design and maintenance of composite airframe structures, it is important to establish damage tolerance of the composites. Currently, the damage tolerance of composites heavily relies on physical testing, due to difficulties of numerical simulation associated with complex damage modes, and prediction of damage progression and strength reductions resulting from LVI. The goal of this study was to develop reliable computational models to simulate the impact damage and predict the damage extent of composites.

A high-fidelity three-dimensional (3-D) finite element (FE) modelling methodology was developed to accurately simulate the damage modes and damage progression in laminated composites during an impact event. To be able to predict different damage modes and their interactions, the cohesive zone modelling (CZM) technique and the LaRC05 failure criteria [1] were employed. To reduce the time required to find the matrix fracture plane angle (α) and the fibre kink band angle (ψ), the Selective Range Golden Section Search (SRGSS) algorithm [2] was used to efficiently find these angles with a 1° precision. The simulation time and the accuracy of the predicted impact responses by the model with the LaRC05 failure criteria with 1° and 5° angle intervals, the model with the LaRC05 with SRGSS algorithm, and the model with the 3-D Hashin criteria [3] were compared. In addition, the ply-by-ply matrix cracking, fibre breakage, fibre splitting, fibre kinking, and interlaminar delamination predicted by the model with the LaRC05 with SRGSS algorithm was presented for a quasi-isotropic composite laminate after a 30 J impact event.

2 MODELLING PROCEDURE

2.1 FINITE ELEMENT MODEL ASSEMBLY

The assembly of the FE model is shown in Fig. 1(a) and (b). A 254 mm by 304.8 mm (10 in by 12 in) carbon/epoxy (IM7/977-3) composite laminate with a stacking sequence of $[0/45/90/-45]_{4s}$ was modelled in Abaqus/CAE. This laminate was impacted by a hemispherical impactor with a diameter of 15.87 mm moving with a kinetic energy at impact of 30 J. The support plate and impactor were considered rigid bodies. Four rubber cylinders were modelled to simulate the clamps, and the rigid body movement of the laminate was constrained in the X and Y (in-plane) directions by defining contacts between the edges of the laminate and three pins of the support plate.

2.2 COHESIVE ZONE MODEL

To predict delamination and intralaminar matrix cracking, cohesive elements with a bilinear traction-separation constitutive relationship were employed between each adjacent composite ply and also inside each ply, as shown in Fig. 1(c). The intralaminar cohesive elements were embedded with a 45° angle to the thickness of the laminate according to the experimental observations [4]. The damage initiation in the cohesive elements was determined by the quadratic stress criterion and the damage evolution was governed by the power law damage evolution criterion [3].

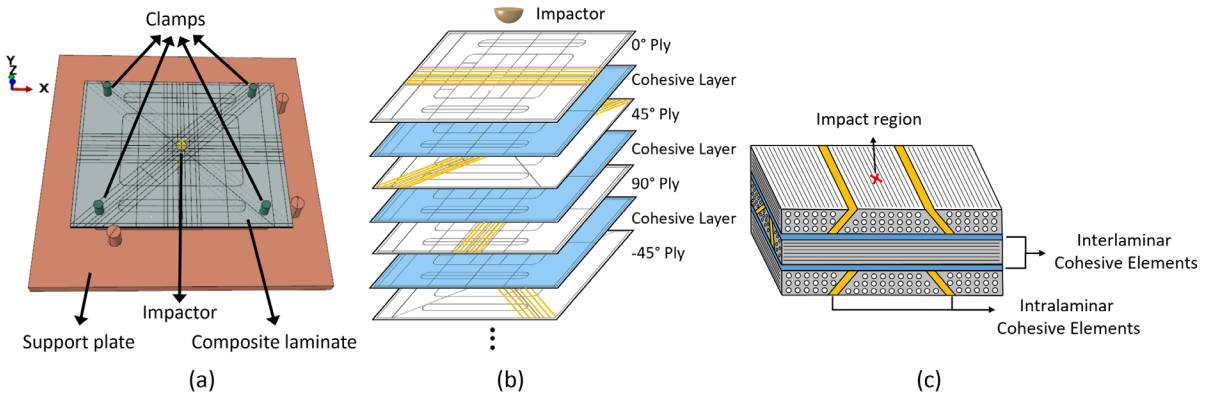

Fig. 1. (a) Assembly of the LVI FE model, (b) Layup configuration, (c) Schematic of the cohesive elements employed in the FE model.

2.3 CONTINUUM DAMAGE MODEL

To predict fibre tensile, splitting, and kinking failures, a VUMAT user-defined subroutine was developed for Abaqus/Explicit based on the LaRC05 failure criteria. This subroutine was also used to capture matrix cracking in regions other than the predefined locations by the intralaminar cohesive elements. The LaRC05 failure criteria consist of four failure modes: matrix failure, fibre tensile failure, fibre splitting failure, and fibre kinking failure. A brief summary of the LaRC05 failure criteria is presented in this section. A detailed explanation of this failure criteria can be found in [1].

To predict the matrix-dominated failure, variations of the Mohr-Coulomb criterion were proposed by Puck et al. [5, 6], and they were shown to be capable of predicting matrix failure under multi-axial stresses. In the LaRC05 failure criteria [1], the Mohr-Coulomb failure criterion was adapted as well for predicting matrix failure in unidirectional composite plies. Using this failure criterion, it is possible to predict the fracture plane angle, which is important for predicting the consequences of failures in composite laminates. The failure index for matrix failure (*FIM*) was defined as Eq. (1):

$$FIM = \left(\frac{\tau_T}{S_T - \eta_T \sigma_N}\right)^2 + \left(\frac{\tau_L}{S_L - \eta_L \sigma_N}\right)^2 + \left(\frac{\langle \sigma_N \rangle_+}{Y_T}\right)^2 \quad (1)$$

Matrix failure happens when $FIM \geq 1$. This criterion is designed for both tensile and compressive matrix failures. The last term in the criterion represents the contribution from the positive normal traction in

the crack opening. In Eq. (1), < > are the Macaulay brackets; S_T and S_L are longitudinal and transverse shear strengths, τ_L, τ_T and σ_N are longitudinal and transverse traction, and normal traction components in the fracture plane, respectively, and can be obtained by stress transformation given in Eq. (2):

$$\sigma_N = \frac{\sigma_2 + \sigma_3}{2} + \frac{\sigma_2 - \sigma_3}{2} cos(2\alpha) + \tau_{23} sin\,(2\alpha)$$
$$\tau_T = -\frac{\sigma_2 - \sigma_3}{2} sin(2\alpha) + \tau_{23} cos\,(2\alpha) \quad (2)$$
$$\tau_L = \tau_{12}\, cos(\alpha) + \tau_{31} sin\,(\alpha)$$

where α is the angle that maximizes FIM and is obtained numerically by evaluating the function at selected angles between 0° and 180°. In Eq. (2), the subscripts of the stresses are showing the directions that are shown in Fig. 2(a). The fracture plane angle for pure transverse compression (α_0) is a material property and can be measured experimentally. For carbon or glass fibre composites α_0 is between 51° and 55° [6–8]. For the material (IM7/977-3) used in the current study, α_0 was set to 53° as suggested in [1]. The friction coefficients η_T and η_L in Eq. (1) are introduced to account for the effects of normal pressure on the failure response. Their effects increase the shear strength in the presence of compressive normal traction and decrease the shear strength in the presence of tensile normal traction. The friction coefficient η_L is a material property and was set equal to 0.082 for IM7/977-3 [1]. The friction coefficient η_T is a function of α_0 and can be calculated using Eq. (3):

$$\eta_T = -\frac{1}{tan\,(2\alpha_0)} \quad (3)$$

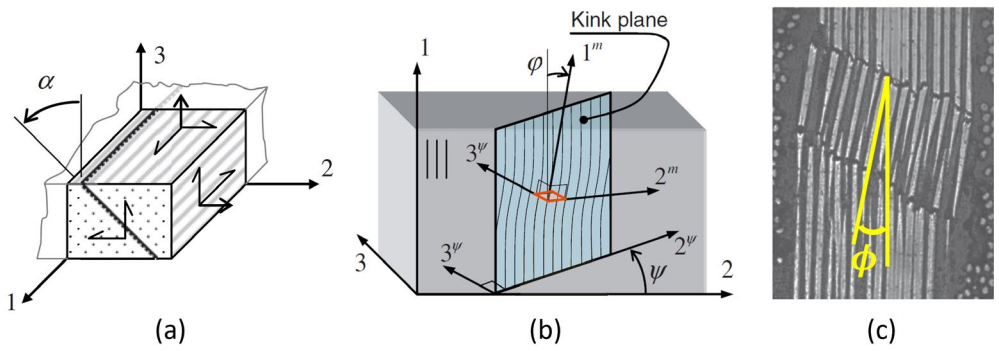

Fig. 2. (a) Schematic of a matrix fracture plane, (b) Schematic of a kink band formation, (c) Micrograph of a kink band formation (reprinted from [1] with modifications).

For predicting the fibre tensile failure, the maximum stress failure criterion was used in the LaRC05 [1]. It has been shown that this simple criterion correlates well with existing experimental data [9]. In Eq. (4), σ_1 and X_T are stress and tensile strength in the fibre direction, respectively:

$$FIT = \frac{\langle \sigma_1 \rangle_+}{X_T} \quad (4)$$

where FIT is the fiber tensile failure index. The physics of fibre compressive failure is less well understood than other failure modes in composite laminates. Kink bands have been observed in different materials and at different scales in the failed material under compressive loading [1]. However, there is no agreement on whether micro-buckling of the fibres or localized matrix failure next to misaligned fibres [10, 11] is the reason for kink band formation. Experimental observations of Pinho et al. [1] showed that a kink band resulting from matrix failure and micro-buckling is not necessarily the triggering factor for this failure mode. Fibre kinking is assumed to result from shear-dominated matrix failure in a misaligned frame under significant longitudinal compressive stress. If the compressive stress in the fibre direction is not significant, the shear-dominated matrix failure in the misaligned frame would result in fibre splitting. Based on experimental observations, Pinho et al. [1] suggested that fibre kinking

only occurs when the magnitude of the longitudinal compressive stress (σ_1) is greater than half of the compressive strength (X_c) in the fibre direction ($\sigma_1 < -X_c/2$), and fibre splitting occurs when longitudinal compressive stress magnitude is lower than half of the compressive strength in the fibre direction ($-X_c/2 < \sigma_1 \leq 0$). In the LaRC05, both failure indices for fibre splitting (FIS) and fibre kinking (FIK) are presented using Eq. (5):

$$FIS = FIK = \left(\frac{\tau_{23}^m}{S_T - \eta_T \sigma_2^m}\right)^2 + \left(\frac{\tau_{12}^m}{S_L - \eta_L \sigma_2^m}\right)^2 + \left(\frac{\langle \sigma_2^m \rangle_+}{Y_T}\right)^2 \tag{5}$$

The rotated coordinate systems relevant for the description of a kink band are shown in Fig. 2(b) and (c). The stresses should be rotated first to the kink-band plane (stresses that are indicated with ψ superscript) and subsequently to the misalignment frame, ϕ, (stresses that are indicated with m superscript). The relevant stress rotation equations for rotation to the kink-band plane are given in Eq. (6):

$$\begin{aligned} \sigma_2^{\psi} &= cos^2\,\psi\,\sigma_2 + sin^2\,\psi\,\sigma_3 + 2\,sin\,\psi\,cos\,\psi\,\tau_{23} \\ \tau_{12}^{\psi} &= \tau_{12}\,cos\,\psi + \tau_{13}\,sin\,\psi \\ \tau_{23}^{\psi} &= -\,sin\,\psi\,cos\,\psi\,\sigma_2 + sin\,\psi\,cos\,\psi\,\sigma_3 + (cos^2\,\psi - sin^2\,\psi)\tau_{23} \\ \tau_{31}^{\psi} &= \tau_{31}\,cos\,\psi - \tau_{12}\,sin\,\psi \end{aligned} \tag{6}$$

The stress rotation equations for rotation to the misalignment frame (ϕ) are given in Eq. (7):

$$\begin{aligned} \sigma_2^{m} &= sin^2\,\phi\,\sigma_1 + cos^2\,\phi\,\sigma_2^{\psi} - 2\,sin\,\phi\,cos\,\phi\,\tau_{12}^{\psi} \\ \tau_{12}^{m} &= -\,sin\,\phi\,cos\,\phi\,\sigma_1 + sin\,\phi\,cos\,\phi\,\sigma_2^{\psi} + (cos^2\,\phi - sin^2\,\phi)\tau_{12}^{\psi} \\ \tau_{23}^{m} &= \tau_{23}^{\psi}\,cos\,\phi - \tau_{31}^{\psi}\,sin\,\phi \end{aligned} \tag{7}$$

The angle of the kink band angle (ψ) should be between 0° and 180° so as to maximize the failure index FIS and FIK. The misalignment angle (ϕ) is the sum of the initial misalignment angle (ϕ^0) due to manufacturing defects and the shear strain (γ_m^0) expressed in a coordinate system aligned with the manufacturing defect:

$$\phi = \frac{\tau_{12}^{\psi}}{|\tau_{12}^{\psi}|}\phi^0 + \gamma_m^0 \tag{8}$$

where γ_m^0 can be obtained using Eq. (9) [7]:

$$\gamma_m^0 = \frac{\phi^0 G_{12} + |\tau_{12}|}{G_{12} + \sigma_{11} - \sigma_{22}} - \phi^0 \tag{9}$$

The initial misalignment angle (ϕ^0) is a material property that can be obtained by the iterative equation given in Eq. (10):

$$\phi^0 = \phi^c - \gamma\left(\frac{1}{2}\,sin(2\phi^0)\,X_C\right) \tag{10}$$

where ϕ^c can be obtained from Eq. (11) [7].

$$\phi^c = arctan\left(\frac{1 - \sqrt{1 - 4\left(\frac{S_L}{X_C} + \eta_L\right)\frac{S_L}{X_C}}}{2\left(\frac{S_L}{X_C} + \eta_L\right)}\right) \tag{11}$$

Using Eq. (10), ϕ^0 was found equal to 2.39° for the material (IM7/977-3) that was used in the current study.

2.4 SEARCH ALGORITHM FOR FRACTURE PLANE AND KINK-BAND ANGLE

In the LaRC05 failure criteria, the matrix fracture plane (α) and the fibre kink band plane (ψ) corresponding to the maximum values of the matrix (FIM) and fibre (FIS or FIK) failure indices need to be identified. To find these planes, the values of the failure indices were calculated by varying both α and ψ angles between 0° and 180°. Without an efficient search algorithm, finding these two angles at every time increment for each finite element would be computationally cumbersome. In the current study, the SRGSS algorithm, which its efficiency and reliability had been tested for Puck's criteria [2], was used for finding both α and ψ. In the SRGSS algorithm, considering that the maximum number of local maxima for failure indices is three and the minimum distance between two local maxima is greater than 25°, the range of angles would be first divided into 18 sections of 10°, as illustrated in Fig. 3. Then, the points with two lower neighbours would be selected as a local maxima, and the range containing these maxima and the two neighbouring points (20° range) should be isolated. Afterward, the iterative golden section search (GSS) algorithm would be applied in each of the maxima-containing ranges to localize the maximum in each range. Finally, the global maximum could be identified. It has been reported [2] that after 6 iterations, the GSS algorithm can find the global maximum with a precision of 1°.

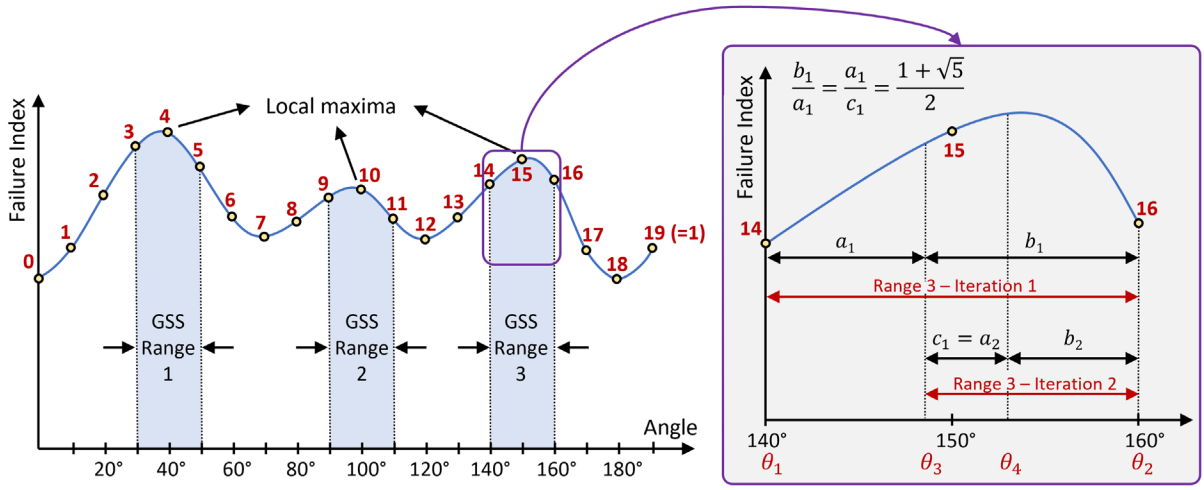

Fig. 3. An example of the selected ranges for the golden section search (GSS) algorithm.

The flowchart of the LaRC05 part of the developed VUMAT subroutine is shown in Fig. 4. This procedure needs to be implemented at each time increment for each element integration point. First, the matrix fracture plane would be found using the SRGSS algorithm and the matrix failure index (FIM) would be obtained on that fracture plane. Afterward, if the stress is tensile (σ_1>0), the fibre tensile failure index (FIT) would be calculated. Otherwise, the fibre kink band angle can be found, and depending on the magnitude of the stress in the fibre direction (σ_1), either the fibre kinking failure index (FIK) or the fibre splitting failure index (FIS) could be calculated. In Fig. 4, θ_1 to θ_4 are the angles that were used in the SRGSS algorithm and are shown in Fig. 3; FIF is the fibre failure index and is equal to FIS or FIK depending on the magnitude of σ_1; "Section_number" is a counter for the angle increments. To account for the possibility that one of the local maxima may occur at 0° (or 180°) the "Section_number" varied from 0° to 190°.

3 RESULTS

In Table 1, a comparison of the computational time is presented between the FE model with the 3-D Hashin failure criteria and that with the LaRC05 failure criteria with different angle intervals for finding α and ψ. The simulation time shown in Table 1 is the time required for the simulation of 8.5 milliseconds of the impact event, which was longer than the contact duration thus enough to model the whole impact event. The VUMAT subroutines were employed with the same FE model and the only difference was

the failure criteria used along with the models. All modes were executed on a high-performance computer (HPC) with 32 CPU cores. The 3-D Hashin scheme was faster than the LaRC05 scheme because of not requiring the matrix fracture plane and fibre kink band angle. It was observed that the LaRC05 scheme with 1° interval was 122% slower than the 3-D Hashin scheme. Even by increasing the angle intervals to 5° the LaRC05 scheme was 24% slower than the 3-D Hashin scheme. By employing the SRGSS algorithm in the LaRC05 VUMAT, the resulting running time became only 14% slower than the 3-D Hahsin scheme. By comparing the LaRC05 with a 1° interval and the LaRC05 with SRGSS failure criteria that have a similar precision, it can be concluded that the SRGSS algorithm made the VUMAT 48% faster.

The predicted impact responses of the composite laminate under 30 J impact were compared with the drop-weight test results in Fig. 5 and Table 2. The maximum displacement was predicted with less than 1% error using each of the FE models. The predicted contact duration with the LaRC05 failure criteria was more accurate with less than 1% error, while the predicted contact duration with the 3-D Hashin failure criteria was 2% higher than the experiment. The peak force was also predicted with less than 8% underestimation with all FE models. A comparison between the key parameters of the predicted impact responses and the experimental results is shown in a radar diagram in Fig. 5. The results of the model with the LaRC05 failure criteria and with 1° angle intervals were almost hidden behind the results of the LaRC05 with the SRGSS algorithm. The reason for this was that both models predicted the matrix fracture and fibre kink band angles with the same precision of 1°. Therefore, the outputs of both models were very similar. However, the model with the SRGSS algorithm was able to give the results in almost half of the time required for the model with 1° intervals.

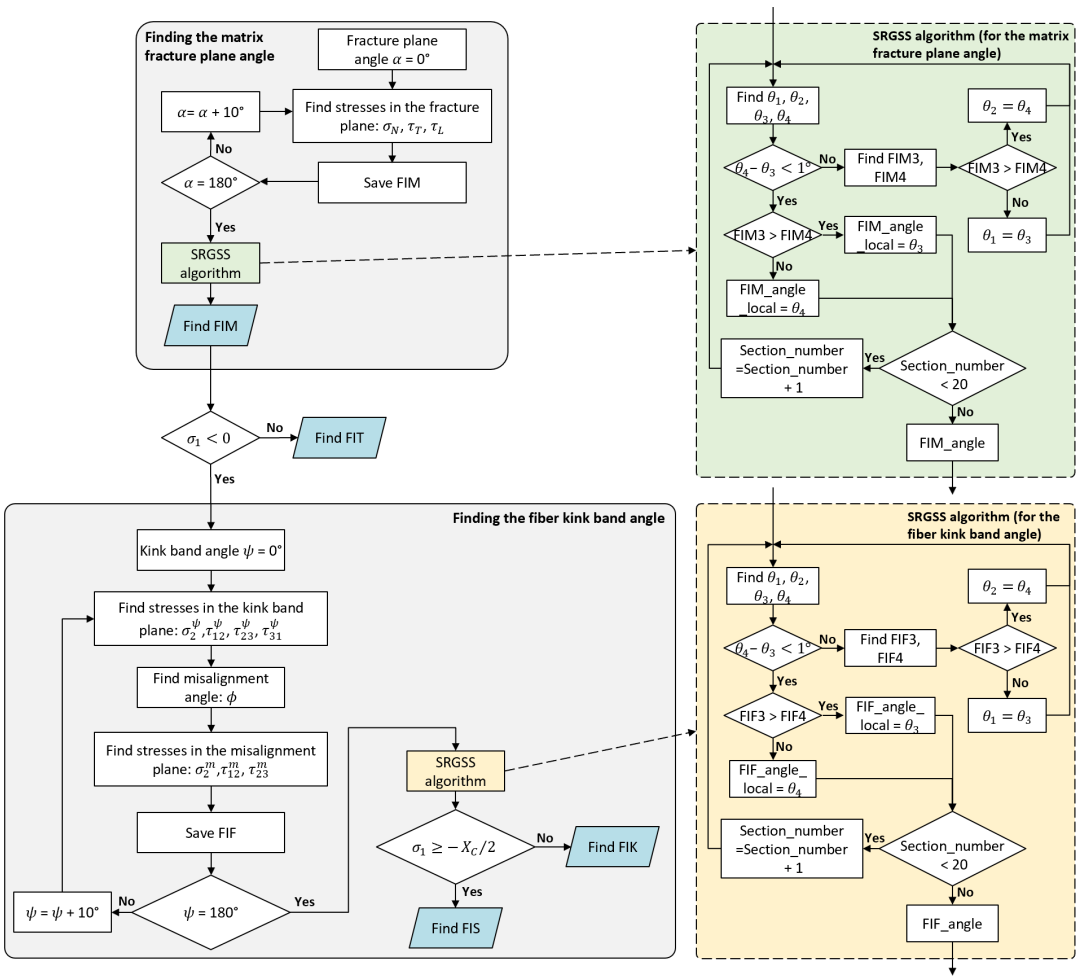

Fig. 4. Flowchart of the VUMAT subroutine with the LaRC05 failure criteria and the SRGSS algorithm.

Table 1. Comparison between the simulation time using the 3-D Hashin and the LaRC05 failure criteria with different angle intervals.

Failure Criteria	Simulation Time (h) ‡	Difference
3-D Hashin	51.2	0
LaRC05 ($\Delta\psi$=1°, $\Delta\alpha$=1°)	113.7	+122%†
LaRC05 ($\Delta\psi$=5°, $\Delta\alpha$=5°)	63.5	+24%
LaRC05 (with SRGSS search algorithm with 1° precision)	58.8	+14%

† Percentage difference of the simulation time compared to the impact FE model with 3-D Hashin failure criteria.
‡ The time required for simulation of 8.5 milliseconds of the impact event.

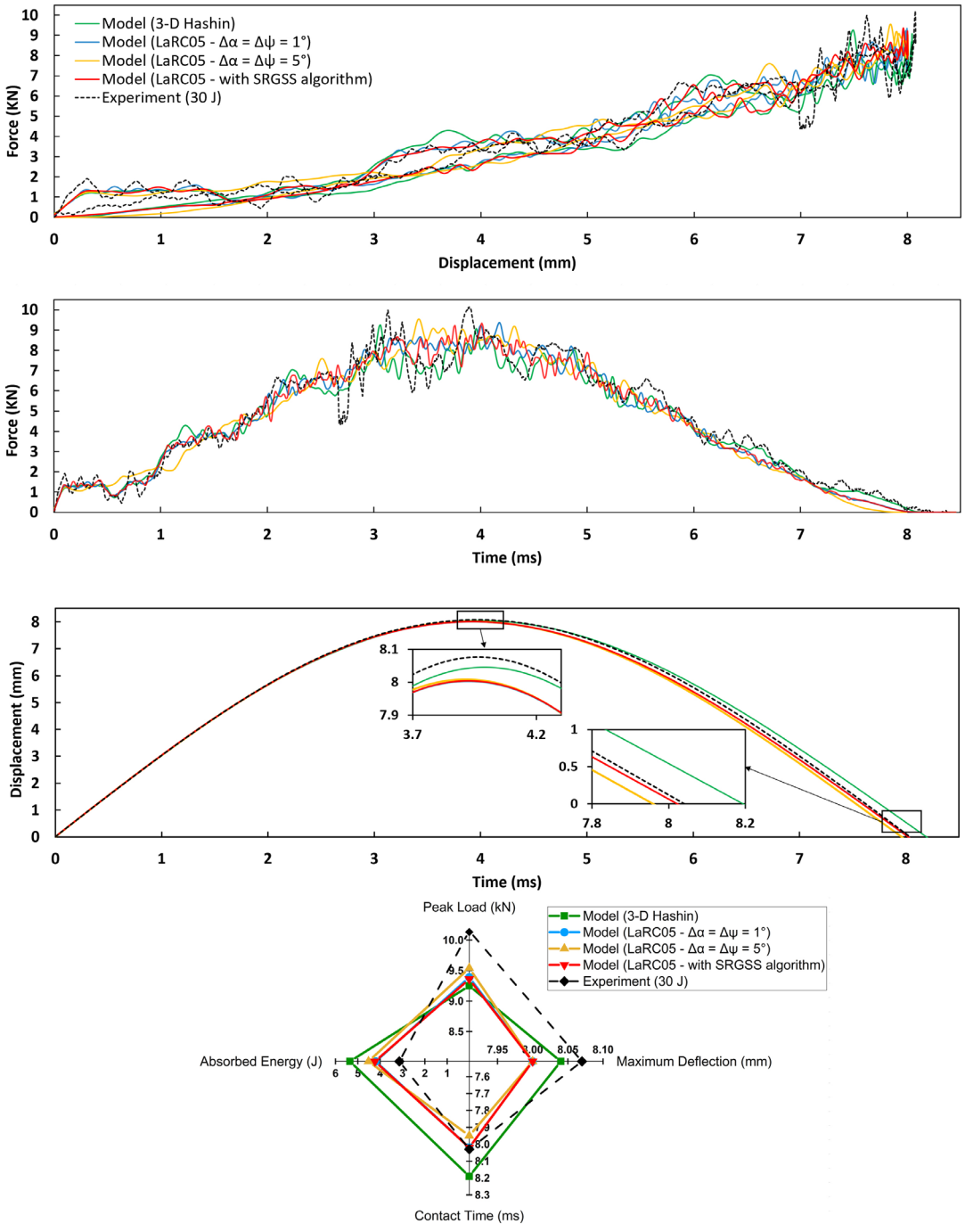

Fig. 5. Comparison between the predicted impact responses and the experimental result.

Table 2. Comparison between the key parameters of the impact predicted responses using the 3-D Hashin and the LaRC05 failure criteria.

	Maximum displacement (mm)	Peak force (kN)	Contact time (ms)	Absorbed energy (J)
3-D Hashin	8.04 (-0.4%†)	9.25 (-8%)	8.19 (+2%)	5.35 (+58%)
LaRC05 ($\Delta\psi$=1°, $\Delta\alpha$=1°)	8.00 (-0.9%)	9.39 (-7%)	8.02 (-0.1%)	4.20 (+24%)
LaRC05 ($\Delta\psi$=5°, $\Delta\alpha$=5°)	8.00 (-0.9%)	9.54 (-6%)	7.95 (-1%)	4.52 (+33%)
LaRC05 (with SRGSS algorithm)	8.00 (-0.9%)	9.34 (-8%)	8.02 (-0.1%)	4.23 (+25%)
Experiment	8.07	10.15	8.03	3.38

† Percentage difference between the predicted and experimental results.

The predicted ply-by-ply damaged areas for the $[0/45/90/-45]_{4s}$ laminate after a 30 J impact event are shown in Fig. 6. The first row shows the matrix cracking. The matrix cracks after a low-velocity impact event would appear either because of the shear stresses near the impacted surface or because of the high tensile stress perpendicular to the fibre direction near the back face of the laminate [3]. The area of the matrix cracking increased from the impacted surface to the back surface. Although the fibre tensile failure index increased as moving from the neutral plane to the back face of the laminate, it did not reach the value of 1 in any of the elements. Therefore, the occurrence of fibre tensile failure was not predicted for the laminate under an impact energy of 30 J. However, fibre splitting and a very small area of fibre kinking were captured near the impacted surface due to high local shear and compressive stresses. It should be noted that there is a difference in the colour of contours used to indicate the state of damage for the delamination and other failure modes. In the last row of Fig. 6, which shows delamination at each interface, the blue colour means that the damage has been initiated and the red colour means that the complete failure has happened and the continuum elements that were sharing the failed cohesive element were completely separated. However, in the other four rows of Fig. 6, which shows the fibre and matrix failure modes, the colours indicate the failure indices and only the red colour means that the failure index reaches the value of one and failure has occurred. Thus, the other elements, which are not red, maintain their initial stiffness.

4 CONCLUSIONS

Using the integrated continuum and discrete damage modelling techniques, both the 3-D Hashin and the LaRC05 failure criteria accurately predicted the impact responses of the selected composite laminates. The model with the LaRC05 failure criteria was 122% slower than the model with the 3-D Hashin failure criteria because of the requirement for finding the matrix fracture plane and fibre kink band angle. However, to predict the consequences of the failures in composite laminates knowing these angles is important. The SRGSS algorithm can be employed along with the LaRC05 failure criteria to reduce the computational time to determine the matrix fracture plane and fibre kink band angle. With using the SRGSS algorithm, the speed of the simulation of an impact event was increased by 48%, and it was only 14% slower than the model with the 3-D Hashin failure that does not require finding the matrix fracture plane and fibre kink band angle.

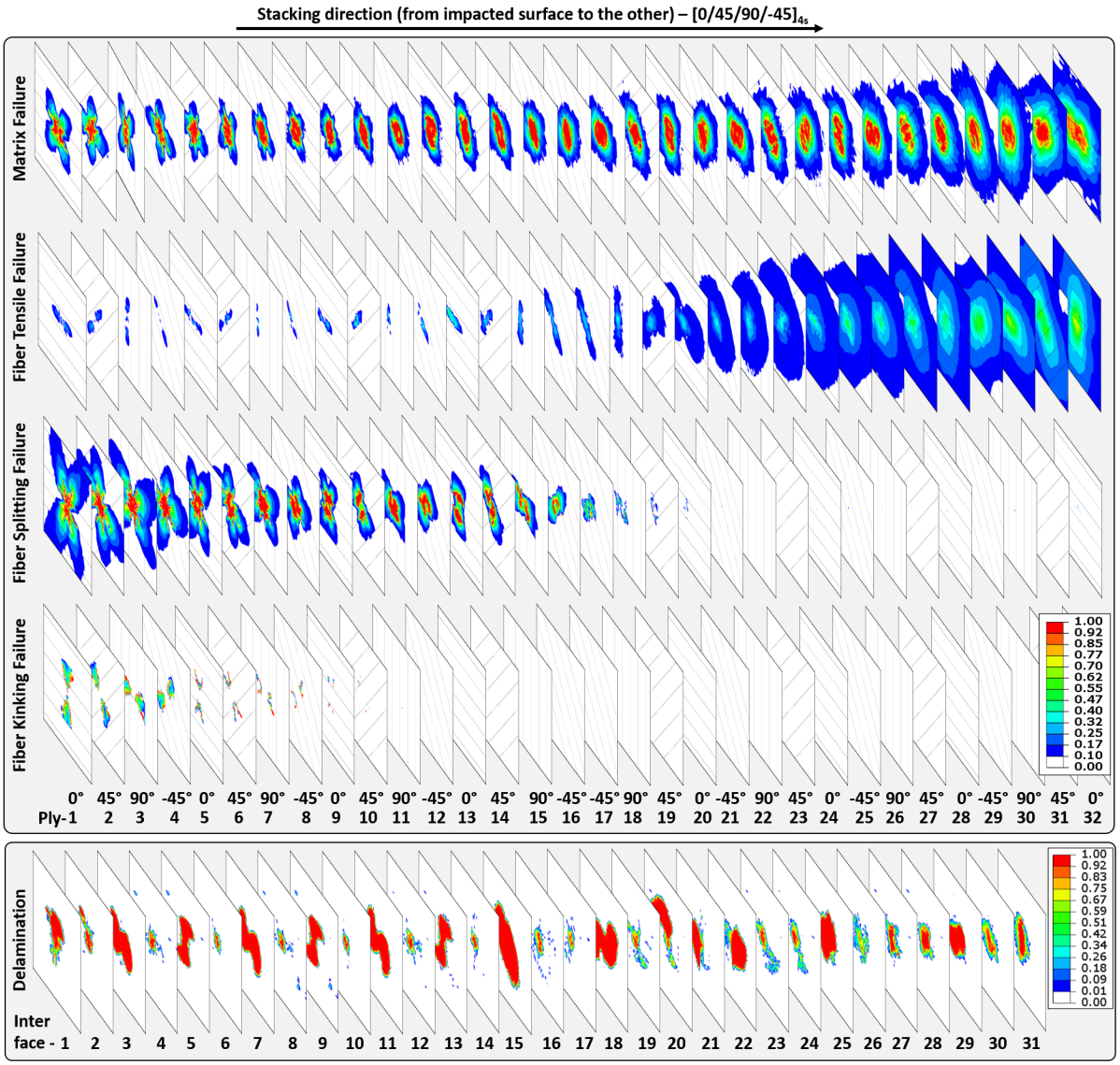

Fig. 6. The ply-by-ply predicted damage areas. Each image shows a 40 mm by 40 mm area surrounding the impacted region.

ACKNOWLEDGEMENTS

The authors would like to thank the Natural Sciences and Engineering Research Council (NSERC) and the Department of National Defence (#DRDC 002) for financial support for this project.

REFERENCES

[1] S. T. Pinho, R. Darvizeh, P. Robinson, C. Schuecker, and P. P. Camanho, "Material and structural response of polymer-matrix fibre-reinforced composites," *Journal of Composite Materials*, vol. 46, no. 19–20, pp. 2313–2341, 2012.

[2] F. J. Schirmaier, J. Weiland, L. Kärger, and F. Henning, "A new efficient and reliable algorithm to determine the fracture angle for Puck's 3D matrix failure criterion for UD composites," *Composites science and technology*, vol. 100, pp. 19–25, 2014.

[3] P. Shabani, L. Li, J. Laliberte, G. Qi, D. Rapking, and D. Mollenhauer, "High-fidelity simulation of low-velocity impact damage in fiber-reinforced composite laminates using integrated discrete and continuum damage models," *Composite Structures*, p. 116910, 2023.

[4] M. McElroy, W. Jackson, R. Olsson, P. Hellström, S. Tsampas, and M. Pankow, "Interaction of

delaminations and matrix cracks in a CFRP plate, Part I: A test method for model validation," *Composites Part A: Applied Science and Manufacturing*, vol. 103, pp. 314–326, 2017.

[5] A. Puck and M. Mannigel, "Physically based non-linear stress–strain relations for the inter-fibre fracture analysis of FRP laminates," *composites science and technology*, vol. 67, no. 9, pp. 1955–1964, 2007.

[6] A. Puck and H. Schürmann, "Failure analysis of FRP laminates by means of physically based phenomenological models," *Composites science and technology*, vol. 62, no. 12–13, pp. 1633–1662, 2002.

[7] S. T. Pinho, C. G. Dávila, P. P. Camanho, L. Iannucci, and P. Robinson, "Failure models and criteria for FRP under in-plane or three-dimensional stress states including shear non-linearity," 2005.

[8] S. T. Pinho, L. Iannucci, and P. Robinson, "Physically-based failure models and criteria for laminated fibre-reinforced composites with emphasis on fibre kinking: Part I: Development," *Composites Part A: Applied Science and Manufacturing*, vol. 37, no. 1, pp. 63–73, 2006.

[9] M. J. Hinton, A. S. Kaddour, and P. D. Soden, "A comparison of the predictive capabilities of current failure theories for composite laminates, judged against experimental evidence," *Composites Science and Technology*, vol. 62, no. 12–13, pp. 1725–1797, 2002.

[10] C. R. Schultheisz and A. M. Waas, "Compressive failure of composites, part I: testing and micromechanical theories," *Progress in Aerospace Sciences*, vol. 32, no. 1, pp. 1–42, 1996.

[11] A. M. Waas and C. R. Schultheisz, "Compressive failure of composites, part II: experimental studies," *Progress in Aerospace Sciences*, vol. 32, no. 1, pp. 43–78, 1996.